Available online at www.sciencedirect.com
SCIENCE DIRECT®
Journal of Electroanalytical Chemistry 554–555 (2003) 307–324
Journal of Electroanalytical Chemistry
www.elsevier.com/locate/jelechem

Electrocatalysis of reformate tolerance in proton exchange membranes fuel cells: Part I

Richard C. Urian, Andrea F. Gullá, Sanjeev Mukerjee *

Department of Chemistry, Northeastern University, Boston, MA 02115, USA

Received 2 October 2002; received in revised form 15 February 2003; accepted 10 March 2003

Dedicated to Professor Michael Weaver and his contribution to surface science and electrochemistry

Abstract

Electrocatalysis of anode electrode tolerance resulting from the presence of both CO and CO_2 in the reformer feed was investigated for Pt, Pt–Ru (1:1) and various atomic ratios of supported Pt:Mo electrocatalysts in proton exchange membrane fuel cells (PEMFCs). In order to elucidate the effects of CO and CO_2 in the reformer feed, separate systematic studies were conducted with varying levels of CO and CO_2 in H_2. The results were used to explain those obtained with a fixed reformate composition: 45% H_2, 10 ppm CO, 15% CO_2, 1% CH_4 balanced with N_2. Results with CO in H_2 showed that PtMo/C exhibits at least a threefold better CO tolerance as compared to PtRu/C and fourfold with respect to Pt/C. The variation of PtMo atomic composition has a negligible effect on CO tolerance. Additional surface poisoning was detected for all the electrocatalysts studied in the molar ratio (H_2:CO_2, 40:60 to 60:40). The presence of a reduced CO_2 species was confirmed using cyclic voltammetry. An ensemble effect was proposed to explain the variation of tolerance to CO_2 as a function of Pt: Mo atomic ratio, this is in contrast to the effect in the presence of adsorbed CO. Interestingly, the overpotential losses in the presence of H_2:CO_2 for PtMo/C (1:1) and PtRu/C (1:1) were very close. As the Pt content of the PtMo/C alloys was increased, the overpotential losses followed those observed for pure Pt, clearly demonstrating a relationship between overpotential loss and Pt site availability. Despite similar overpotential losses between Pt/C and PtMo/C (5:1), both of which were greater than PtRu/C (1;1) the overpotential loss observed for PtMo in a CO_2+CO reformate mix was far better than for both PtRu/C and Pt/C.

Keywords: Reformate tolerance; Electrocatalysis; Proton exchange membrane fuel cells; PtMo; Reverse shift reaction

1. Introduction

Proton exchange membrane fuel cells (PEMFCs) are currently attractive candidates for low emission power sources for both stationary and portable applications. In this endeavor, the systems closest to commercialization are those which include on-board reformation of a fuel such as methanol, natural gas or even gasoline for hydrogen production. This steam reformation process is typically followed by clean up steps, which include the high and low temperature shift converters and a selective oxidizer (called the 'prox' unit) for lowering the CO content of the reformer outlet. Typical levels of CO at the inlet stream of a PEMFC are expected to be in the range of 50 and 100 ppm. Besides CO, the major constituent of the reformate gas outlet is CO_2. The levels of CO_2 however can vary between 35 and 40% (dry gas composition) for the high temperature iso-octane system (gasoline) and 75% (dry gas composition) for the relatively low temperature methanol reformation [1]. The anode feed stream, therefore, typically contains a mole fraction of hydrogen in the range of 0.4–0.75, with CO in the range of 50–100 ppm and CO_2 making up the balance.

The presence of CO as a poison in the anode feed stream together with hydrogen has been well documented and a large body of literature is available, both for

* Corresponding author. Tel.: +1-617-373-2382.
E-mail address: smukerje@lynx.neu.edu (S. Mukerjee).

0022-0728/03/$ - see front matter © 2003 Elsevier B.V. All rights reserved.
doi:10.1016/S0022-0728(03)00241-9

PEMFCs as well as for the medium temperature phosphoric acid systems. However, the presence of CO_2 and its effect has not yet been examined in detail. There is very limited literature available in the public domain on the possibility of a reverse shift reaction of CO_2 (reduction) to produce CO at the typical PEMFC operating temperature of 80 °C. For the higher temperature phosphoric acid fuel cell (PAFC) system, the presence of CO_2 is largely considered as a diluent (96% H_3PO_4 at 160 °C) [2]. One of the earliest reports on CO_2 reduction at low temperatures was presented by Giner [3]; it was shown that in acid solutions (H_2SO_4) CO_2 is reduced by chemisorbed hydrogen in the potential range of 0–250 mV (vs. RHE). The activation energy was determined to be 92 kJ mol^{-1}. Giner, also indicated that the adsorbed CO_2 formed was what he called a reduced CO_2 species (hereby referred to as 'CO_2') on the Pt surface. This 'CO_2' species was similar to those formed in the presence of partially oxygenated fuels such as methanol [4] and saturated hydrocarbon [4]. Early investigations focussing on the identification of the type of species formed have suggested the formation of carboxylic type moieties on the Pt surface [5]. Also reported was the surface coverage (θ) on a platinized surface for 'CO_2' which was approximately 0.7 at 40 °C with the charge for oxidation of the adsorbed 'CO_2' per one adsorption site being equal to one. Similar results were also reported by Kamath and Lal [6]. Stonehart [7] suggested a two electron oxidation process for the adsorbed 'CO_2' species and reported a higher rate constant for 'CO_2' as compared to CO mono-hydrate.

A number of reports have appeared on the different species of adsorbed CO and 'CO_2' (see Ref. by Sobkowski and Czerwinski [8]) most of which agree on a two-electron oxidation for reduced 'CO_2'. The general consensus is that, based on the electrode potential, different species are formed by CO and CO_2. For example at low potentials, where Pt is covered by adsorbed hydrogen (Pt–H_{ads}), CO forms both linear and bridge bonded CO species. This observation is also confirmed by prior in situ IR spectroscopy (EMIRS technique) by Beden and coworkers [9,10] and Lamy et al. [11]. Moreover, the ratio of linear and higher coordinated forms (such as bridge bonded) appears to be a function of electrode potential. Adsorption of CO_2 on the platinum surface is expected to occur mainly in the potential range where surface adsorbed hydrogen on Pt is present (hence in the low potential hydrogen region [12–14]. These prior studies were mostly conducted in aqueous electrolytes such as H_2SO_4 at or just above room temperature.

The poisoning effect of a supported Pt electrocatalyst due to the presence of CO_2 in the anode gas input has been presented [15,16] for PEMFCs; moreover, such an effect was also investigated in a recent report on PEMFCs operating at 65 °C under ambient pressure conditions [17]. In this work, an additional overpotential loss of $\sim$20 mV at 400 mA cm^{-2} was reported and it was ascribed to the presence of 21% CO_2 in the reformate output (dry gas composition: 21% CO_2, 30% N_2, balance H_2). Such a result, if translated to interfacial resistance, correlates to a 70–90 mA cm^{-2} loss in the linear region of the polarization curve.

The current state of the art electrocatalyst for reformer fed anode electrodes in PEMFCs is PtRu/C. The CO tolerance (with an economically viable electrocatalyst loading, 0.1–0.4 mg cm^{-2}) at low levels (<20 ppm) is acceptable. However, higher CO levels such as those in the 100 ppm range result in a significant overpotential loss (200–250 mV at 0.7 A cm^{-2}). Presently, air bleeding in the anode feed stream is used to mitigate the CO poisoning problem; however, a more elegant solution would be an improved tolerance to both CO and CO_2.

In this context, recent and promising results [21,22] with PtMo/C have been shown, some of which report up to a threefold enhancement in performance with H_2 (100 ppm CO)/O_2 as compared to PtRu/C. Improvement in CO tolerance relative to PtRu/C has also been observed for supported PtW and PtCoMo [18,19]. However, there has been very limited work on the effect of CO_2 present in the reformer output stream to the fuel cell, especially with binary alloy electrocatalysts such as PtRu/C and PtMo/C. A recent short communication [20] has compared the effect of CO_2 in the anode feed of a PEMFC, between PtMo/C and PtRu/C with the atomic ratio of the alloys being 77:23 and 51:49, respectively; Pt/C was used as a control. In this report, the CO tolerance to a H_2/CO mixture (10–100 ppm) was superior for PtMo/C as compared to PtRu/C and in agreement with prior reports [21]. However, in the presence of CO_2 (25% dry gas composition, balance H_2), an additional overpotential loss of 500 mA cm^{-2} (80 °C cell temperature) was reported for PtMo/C relative to Pt/C while PtRu/C maintained a slightly better tolerance as compared to Pt/C.

The present work is aimed at comparing the performance of a series of carbon supported PtMo electrocatalysts with Pt (control), and Pt:Ru (1:1 atomic ratio a/o) in a typical reformer fed fuel cell. The objective is to provide a systematic qualitative picture of the overpotential losses as a result of varying amounts of CO_2 in the reformate feed to the anode. For this, a range of ratios of CO_2 to H_2 has been used to examine the additive nature of the surface poisoning on the PtRu/C and PtMo/C as compared to the control Pt/C. The goal was to draw distinctions between the poisoning effect of CO and CO_2 as a function of composition of the electrocatalysts (choice of the alloying element, atomic ratio and the methodology of preparation).

2. Experimental

2.1. Electrocatalyst and electrode specifications

Three types of carbon-supported Pt based electrocatalysts were used in the anode electrodes. These comprised of 30% Pt/C, 30% PtRu (1:1 a/o) and four different compositions of 30% PtMo/C (1:1, 3:1, 4:1 and 5:1, Pt:Mo a/o). The choice of PtRu/C (1:1) was based on the fact that it is the most widely used electrocatalyst for reformate tolerant anode electrodes. The four different compositions of PtMo were used to determine the influence of the Pt:Mo atomic ratio on the tolerance of CO_2. Among these compositions, the data for 5:1 a/o PtMo/C is reported in greater detail because this composition allowed a maximum Pt to Mo ratio and hence the greatest susceptibility to CO_2. The other compositions were used to understand the level of CO_2 tolerance in the context of the PtRu/C (1:1a/o) and Pt/C (control). All electrocatalysts used in this investigation were obtained from De Nora N.A., E-TEK division, Somerset, NJ with the exception of PtMo/C (1:1). This catalyst was synthesized in-house. In order to verify our synthesis methodology, all of the PtMo/C compositions obtained from De Nora N.A., E-TEK division, Somerset, NJ were also prepared in-house. Comparison of the two sets of catalysts exhibited very close performance characteristics.

The cathode electrode was the same in all experiments (a Pt/C electrode with 20% Pt on C, loading of 0.4 mg cm^{-2} from De Nora N.A., E-TEK division, Somerset, NJ). The anode electrodes were made in-house with a metal loading of 0.4 mg cm^{-2}, using a spraying process and a non catalyzed single sided ELAT electrode from De Nora N.A., E-TEK division. The MEA was fabricated in-house with Nafion®1135 (1100 MW and 3.5 mill) using a standard in-house hot pressing technique. Nafion® loading in the MEA was approximately 0.6 mg cm^{-2}.

2.2. Physico-chemical characterization

X-ray diffraction was conducted using the high resolution X-18A beam line at the National Synchrotron Light Source (NSLS) at Brookhaven National Laboratory. The previously reported characterization of the 3:1 and 4:1 PtMo/C composition [22] showed the existence of a fcc metallic phase with an average particle size of ca. 4 nm. Since the lattice constants for the PtMo solid solutions are very close to that of pure Pt, the compositions of the nanocrystalline phase could not be determined. Within the limits of this technique, however, no separate phases associated with Mo, e.g. metal oxide, or carbide were detected, suggesting thereby that most if not all of the Mo was alloyed to the Pt. TEM analyses of the as-received electrocatalysts were conducted using a JOEL transmission electron spectrometer (model 3010) operating at an energy of 200 kV. Electron diffraction data was also obtained for every sample. Line broadening analysis of the primary XRD peak $\langle 111 \rangle$ was conducted using the Scherrer treatment of the data. The data were first fitted to an indexing program, which allowed accurate measurement of the line widths at half maximum. These widths were then used to obtain the particle size. Corrections for beam deviations in the instrument were considered negligible due to the high collimation of the synchrotron beam.

In addition, X-ray absorption near edge structure (XANES) data from in situ X-ray absorption spectroscopy (XAS) was measured. The objective was to verify the nominal atomic ratios provided by the vendor as well as the nature of alloying, especially in the case of PtMo/C where the difference in the line shifts of the XRD patterns were very small even with the high resolution synchrotron radiation source. The XAS spectra, with its two complimentary spectral components, the near edge region, XANES and the extended part, X-ray absorption fine structure (EXAFS) provide information on the changes in both electronic (Pt d-band vacancy/atom) as well as short range atomic order (bond distances, coordination numbers, etc.). The advantages of this technique are its element specificity and in situ capability. For the purpose of determining the atomic ratio a special in situ spectro-electrochemical cell (described in detail elsewhere [23]) was used, which allowed XAS measurements in transmission mode with the working electrode in a totally flooded state. XAS measurements were conducted at beam line X-11A at the National Synchrotron Light Source (NSLS) in Brookhaven National Laboratory, with the storage ring operating at 2.8 GeV and a current between 350 and 120 mA. Data were collected at both the Pt L (L_3 and L_2) and Ru and Mo K edges in the transmission mode using a three detector set up comprising of the incident and transmitted beams and a reference. The reference detector provided accurate calibration and alignment of the edge positions, for which a pure standard foil ($\mu x = 1$) of the element edge being probed was employed. Details of the beam line optics and the monochromator are given elsewhere [24]. The monochromator, (Si 111 crystals) was detuned by 15% for the Pt L edges and 10% for both the Mo and Ru K edges, respectively, to reject higher harmonics.

In situ XAS data for all electrocatalysts (at the Pt L and alloying element K edges) for the purpose of XANES analysis were measured at 0.54 V versus RHE using a computer interfaced potentiostat/galvanostat (PGSTSAT 30, Autolab, Echochemie, Brinkmann Instruments). The electrolyte choice was 1 M $HClO_4$. Prior to acquiring the in situ XAS spectra, electrodes were cycled between 0.0 and 0.65 V at least 25 times, the choice of the upper potential cutoff was to avoid

possible dissolution of Mo and Ru. Since the purpose of the XAS experiment was primarily to determine the atomic ratio of Pt and the alloying element, the in situ spectra were taken at 0.54 V versus RHE. Data collected at this potential were devoid of interference due to adsorbed species, being in the double layer region and close to the potential of zero charge. Detailed EXAFS analysis at this potential using the Pt L_3 edge data is presented elsewhere [25].

2.3. Electrochemical characterization

All membrane electrode assemblies (MEAs) were tested in a 5-cm^2 single cell fuel cell (Fuel Cell Technologies, Albuquerque, NM) using a locally constructed test station facility for steady-state polarization measurements. This test station allowed independent control of humidification, cell temperature, gas flow rate, etc. The single cell design incorporated reference electrodes, which allowed simultaneous measurement of the anode and cathode half-cell polarization along with the single cell data. Polarization data were acquired using a LabView® routine, written in-house. The program was interfaced with a HP 60508 Electronic Load main frame, which housed a HP 60501B 150 W electronic load module.

All MEAs were conditioned prior to testing using a series of steps. The initial step involved a slow ramp of the cell temperature from room temperature to 85 °C (approximately 2 °C h^{-1}) with saturated N_2 flow on both electrodes. After keeping the cell under these conditions for approximately 5 h, the pressure was slowly increased to 50/60 psig anode/cathode respectively. The gases were switched to saturated H_2 and O_2 with the cell allowed to equilibrate for a couple of hours. Humidification conditions were checked by monitoring the cell backpressure and inlet gas temperatures. Following this conditioning step all MEAs were initially tested with H_2/O_2 measuring simultaneously the single and half-cell polarization. Half-cell cathode polarizations for all MEAs were compared to the control (Pt/C electrodes, anode and cathode). Only those MEAs which exhibited less than ± 5 mV variation at 1 A cm^{-2} for the cathode half cell data were used for subsequent measurements.

The operating conditions for all fuel cell tests were: cell temperature 85 °C, 100% relative humidification, cathode side gas was oxygen and the anode gas compositions were (i) H_2, (ii) H_2+N_2 and (iii) H_2+CO_2. Both (ii) and (iii) gas mixtures were taken in the ratios of 60:40, 50:50, 40:60 molar ratios. In addition, the steady-state polarization measurements were also measured with anode gas compositions containing (i) 5, 20, 50 and 100 ppm of CO (balance H_2) as well as (ii) reformate mixture of 45% H_2, 10 ppm CO, 15% CO_2, 1% CH_4 balanced with N_2. The cyclic voltammograms were obtained using an Autolab potentiostat/galvanostat (PGSTAT-30, Ecochemie, Brinkman Instruments) with software package. Cyclic voltammetry was performed on all the MEA systems while still in the single cells, after all polarization tests had been completed. This involved passing pure H_2 over the reference and counter electrode chamber (cathode electrode) and N_2 over the working electrode (anode electrode). In addition, cyclic voltammograms were also measured with pure CO_2 flowing in the working electrode chamber (anode electrode) instead of N_2.

All data reported in this paper are an average of at least three separate polarization measurements, within each set of data, variations were always less than ± 4–5 mV at 500 mA cm^{-2}. In addition each electrocatalyst was tested at least as two separate MEAs to ensure reproducibility.

2.4. Kinetic model for CO_2 poisoning and dilution effects

As mentioned in the introduction section, the aim of this report is to provide a systematic and quantitative picture of the overpotential losses due to the presence of varying amounts of CO_2 in the reformate feed-stream. A detailed kinetic model for examining this effect has been formulated and it is the subject of a different publication. In this report, a part of this model has been used to determine the level of CO coverage on the electrocatalysts surface, resulting from the reverse water gas shift reaction (conversion of CO_2 to CO). Such a conversion process can be written in accordance to two reaction pathways [3]: (i) $CO_2+H_2 \rightleftarrows CO+H_2O$ (known as the reverse water gas shift reaction) and/or (ii) $CO_2+2H^++2e^- \rightleftarrows CO+H_2O$ (known as the electro-reduction reaction). The effect of either in terms of the effect of surface coverage and its effect on overpotentials will be the same. Hence CO is expected to be produced at the interface, whenever there is adjacent CO_2 and H_2 adsorption and consequently the overpotential losses will depend upon the various H_2+CO_2 mixtures. At the rather low operational temperatures, typical to PEM fuel cells, the poisoning effect of CO will be more pronounced as compared to the CO_2 dilution effects. Further, this reverse shift process is likely to occur only in the forward direction; because under the operational conditions, the rate of the forward reaction is higher when compared to the rate of the reverse reaction. The equilibrium concentrations can be calculated as follows:

$$n_{CO_2,in}CO_2 + n_{H_2,in}H_2 + n_{H_2O,in}H_2O \rightarrow n_{CO_2,out}CO_2 + n_{H_2,out}H_2 + n_{H_2O,out}H_2O + n_{CO,out}CO$$

$$k_P = \frac{P_{CO_2,out} \cdot P_{H_2O,out}}{P_{H_2,out} \cdot P_{CO_2,out}} \quad (1)$$

The steady-state model presented here for the under-

standing of CO poisoning on the catalyst surface of the Pt-alloys is based on a four step kinetic process and on a previous analytical discussion of the problem proposed in an earlier work by Springer et al. [26] The model assumes that the ionic resistance of the catalyst layer is low enough to neglect any potential changes across the catalyst layer. In the context of this investigation, poisoning due to the formation of 'reduced CO_2' species is studied as a function of different H_2:CO_2 concentrations.

$$\mathrm{CO} + \mathrm{M} \underset{b_{\mathrm{fc}}(\theta_{\mathrm{CO}})k_{\mathrm{fc}}}{\overset{k_{\mathrm{fc}}}{\rightleftarrows}} (\mathrm{M}-\mathrm{CO}) \qquad [1]$$

$$\mathrm{H_2} + 2\mathrm{M} \underset{b_{\mathrm{fh}}k_{\mathrm{fh}}(\theta_{\mathrm{CO}})}{\overset{k_{\mathrm{fh}}(\theta_{\mathrm{CO}})}{\rightleftarrows}} 2(\mathrm{M}-\mathrm{H}) \qquad [2]$$

$$2(\mathrm{M}-\mathrm{H}) \overset{k_{\mathrm{eh}}}{\rightarrow} \mathrm{H^+} + \mathrm{e^-} + \mathrm{M} \qquad [3]$$

$$\mathrm{H_2O} + (\mathrm{M}-\mathrm{CO}) \overset{k_{\mathrm{ec}}}{\rightarrow} \mathrm{M} + \mathrm{CO} + 2\mathrm{H^+} + 2\mathrm{e^-} \qquad [4] \qquad (2)$$

In Eq. (2), which refers to a sequence of steps (1–4), M represents the metal considered for the system under investigation. The first two steps in Eq. (2) are both occurring on the catalyst surface layer and represent the two competing steps of the kinetics; step (1) denotes the CO adsorption and step (2) corresponds to the dissociative chemisorption of H_2. The third step in Eq. (2) represents the current density corresponding to the anodic H_2 oxidation. The last step in Eq. (2) denotes the electrochemical oxidation of CO to CO_2. Moreover, the forward rate constants, for both the hydrogen (k_{fh}) and CO (k_{fc}) adsorption, are expressed in units of A cm^{-2}, while the ratio of the backward-to-forward rate constants are expressed in units of atmosphere (atm). Both the desorption rate for CO and the adsorption rate for hydrogen are assumed to be a function of CO coverage, while the ratio of adsorption/desorption rate for hydrogen and the adsorption rate for CO are considered to be constant with CO coverage.

It is well recognized that the rate determining step in the case of CO oxidation is the formation of surface oxide and oxyhydroxides from the anodic water activation step; this corresponds to step 4 presented in Eq. (2).

3. Results and discussion

3.1. Characterization of the nano-cluster size and morphology: powder XRD, TEM and in situ XAS measurements

Detailed characterization of the nanocluster size and morphology is essential for understanding of the true importance of the electrochemical data. A representative TEM picture of the PtMo/C (5:1 a/o) from ETEK is shown in Fig. 1. The corresponding electron diffraction pattern is also shown. Analysis of the TEM pictures for other electrocatalysts in terms of their particle size is given in Table 1. The average particle size obtained from TEM analysis ranges between 30 to 35 Å. The dispersion of the electrocatalysts was excellent with a very narrow distribution of particle size (within 15 Å for all the electrocatalysts). XRD analysis of the electrocatalysts showed a very high degree of crystallinity. Fits of the XRD data to an indexing routine showed that all the patterns (Pt and Pt alloys) corresponded to a fcc lattice. The lattice parameters obtained are given in Table 1. In addition, the Pt–Pt bond distances based on a fcc lattice were calculated (Table 1). As is evident from the data, alloying of Pt with Ru and Mo results in a lowering of the lattice parameters (and hence the Pt–Pt bond distance). While the perturbation of the lattice parameter for PtMo/C was negligible, those for PtRu/C were significant. Here the Pt–Pt bond distance is lowered by approximately 0.026 Å. As pointed out in Section 2, the

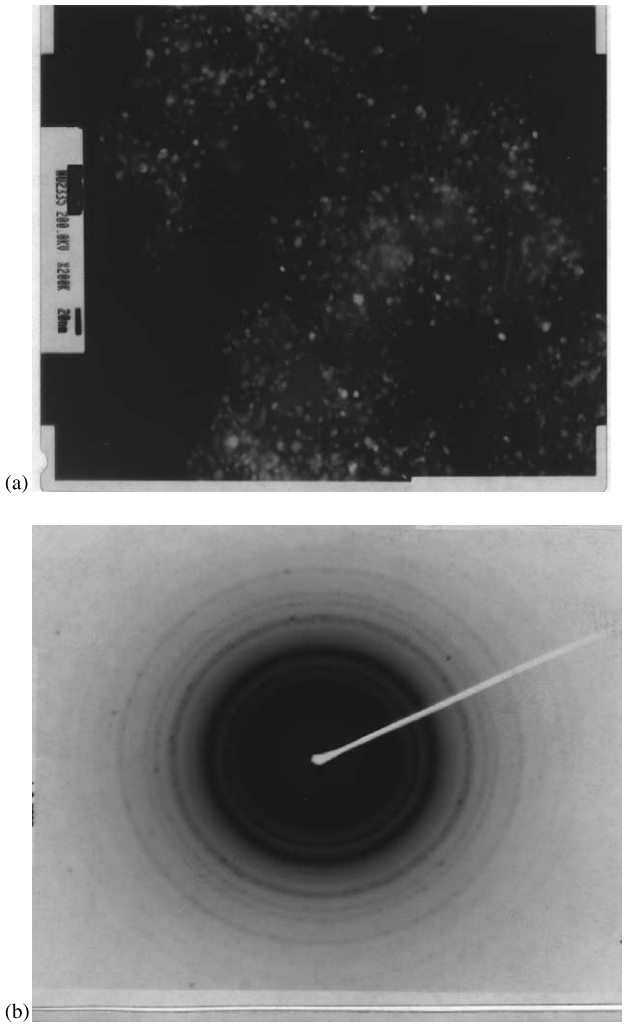

Fig. 1. (a) TEM image and (b) electron diffraction pattern for the PtMo/C (3:1 atomic ratio, Pt:Mo) electrocatalyst (as received).

Table 1
Results of TEM, XRD and in situ XANES spectroscopy on PtRu/C (1:1 a/o), Pt/C and different alloying compositions of PtMo/C (5:1; 4:1; 3:1 and 1:1 a/o)

Electrocatalyst	Nominal atomic ratio (a/o)* metal loading/C/%	Atomic ratio (from XANES) Pt/M/%	XRD analysis		Particle size/Å	
			XRD lattice parameter/Å	Pt–Pt bond distance/Å	X-ray line broadening analysis	TEM
Pt/C	– 20	–	3.927	2.777	28	30
PtRu/C	1:1 30	62:38	3.8905	2.751	35	35
PtMo/C	5:1 30	84:16	3.9255	2.776	31	31
PtMo/C	4:1 30	78:22	3.9212	2.773	33	35
PtMo/C	3:1 30	72:28	3.9145	2.768	32	31
PtMo/C	1:1 30	65:35	3.9105	2.765	35	34

The in situ XANES data is taken at both the Pt L_3 and alloying element K edge at 0.54 V vs. RHE. All alloying compositions are expressed in atomic percent ratio (a/o) of Pt:M, where M is the alloying element.

XRD pattern for PtMo/C was very close to that of Pt/C, hence a strong conclusion on alloy formation was not possible. As shown in Table 1, the lattice parameters were very close to that for Pt/C, hence a negligible change in the Pt–Pt bond distance as compared to Pt/C. The electron diffraction patterns for Pt/C and PtMo/C were also very close. The particle size obtained from using the ⟨111⟩-diffraction line broadening analysis showed remarkable agreement with the corresponding TEM data. The particle sizes obtained were all in the range of 28–35 Å.

XANES analysis at the Pt L and alloying element K edge at 0.54 V involved measurement of edge jumps in the transmission mode. Analysis using methodology described in detail elsewhere [23,25,27] provided Pt and alloying element loading in mg cm^{-2}, which was then converted to the atomic ratios given in Table 1. These atomic ratios were in reasonably good agreement with the specified nominal loading of the electrocatalyst. Detailed analysis of the EXAFS at the Pt L_3 edge on these PtMo/C alloys has been reported recently [28]; this analysis has confirmed the alloy formation in the PtMo/C electrocatalysts. Confirmation of alloying was evident from both the perturbation of the short-range atomic order (Pt–Pt bond distance and coordination numbers) as well as the increase in the Pt d-band vacancy/atom due to alloying with Mo or Ru.

It is interesting to note that with the exception of the 1:1 atomic ratio of Pt:Mo, other compositions show very good agreement between results of XANES analysis and the nominal composition given by the manufacturer (De Nora N.A., E-TEK division, Somerset, NJ). XANES analysis of the 1:1 composition shows the actual ratio to be 65:35 (Pt:Mo). The most probable reason for this discrepancy is based on the limit of solubility of Mo in the Pt, which according to prior reports [29,30] is approximately $\sim$27 a/o. This limit of solubility is however controversial with somewhat higher values reported elsewhere [31].

3.2. Electrochemical characterization: dynamic and steady-state measurements

In order to understand reformate tolerance, the interaction of both CO and CO_2 with the catalyst surface has to be investigated. For CO tolerance, the key parameters are the work function of the surface for CO adsorption and its oxidation using surface oxides. In contrast the poisoning (if any) due to reverse shift reaction with CO_2 to produce CO requires the presence of surface H_2 and available active surface reaction centers, the most favored surface being bare Pt. In order to understand reformate tolerance better, this section examines the surface interaction of both CO and CO_2 on these different electrocatalysts.

Fig. 2 shows the single cell polarization curves for carbon supported Pt, PtRu (1:1) and PtMo (5:1) electrocatalysts at 85 °C, 60/50 psig backpressure for cathode and anode electrodes respectively (100% humidification condition) with both H_2 [100 ppm CO]/O_2 and reformate/O_2 (reformate composition: 45% H_2, 10 ppm CO, 15% CO_2, 1% CH_4 balanced with N_2). Comparison with the H_2/O_2 polarization curve up to a current density of approximately 1 A cm^{-2} shows that the primary contribution to the kinetic losses is due to the presence of reformate gases, (most significantly CO). The contributions due to mass transport polarization are negligible and the extent of ohmic polarization losses are approximately the same for all the MEAs tested up to 1 A cm^{-2} current density. A more accurate evalua-

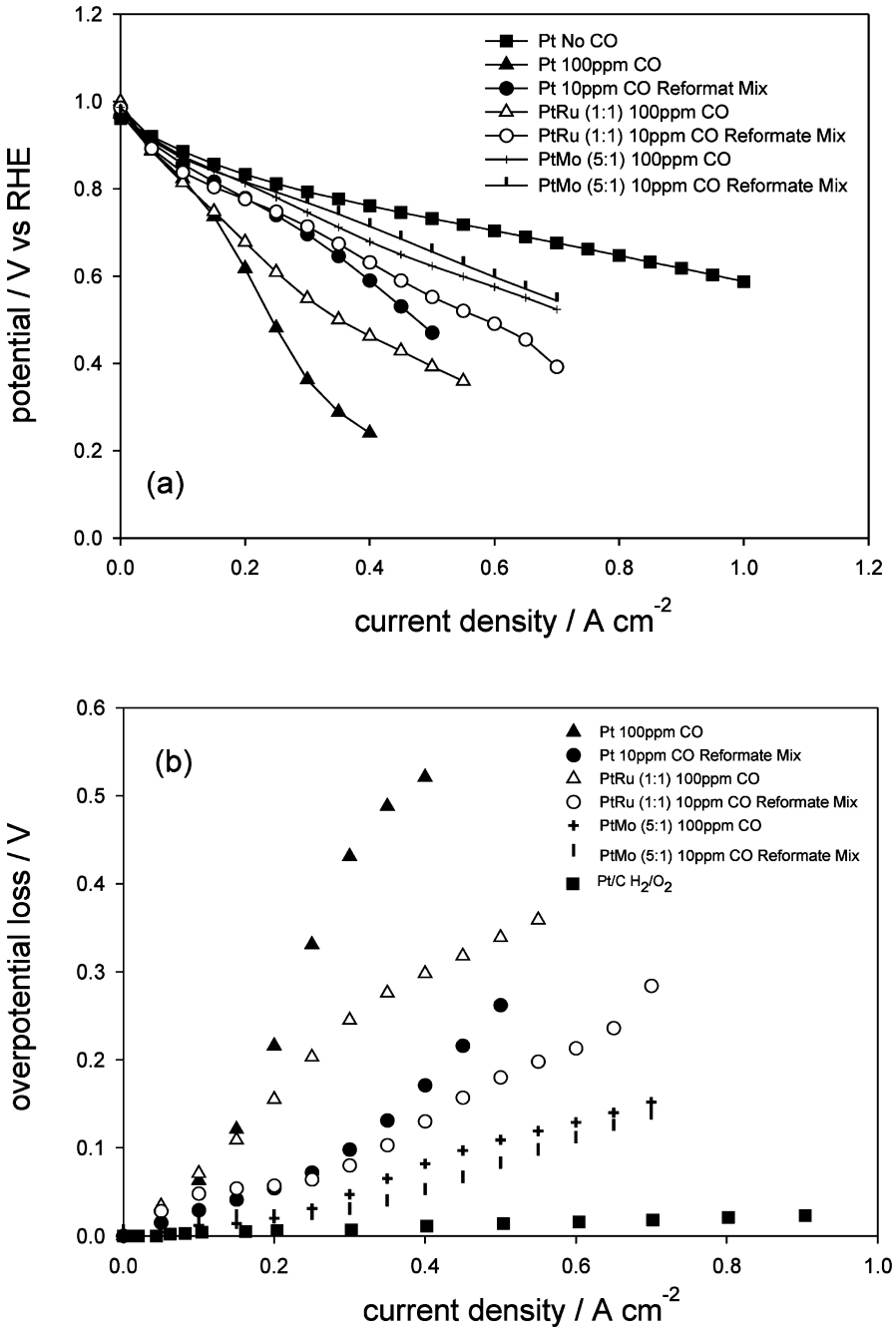

Fig. 2. Steady-state polarization data from PEM fuel cells as a function of different anode gas feeds, H_2 [100 ppm CO]: Pt/C (▲), PtRu/C {1:1 atomic ratio} (△) and PtMo/C {5:1 atomic ratio, Pt:Mo} (+) and H_2 [10 ppm CO+reformate mixture]: Pt/C (●), PtRu/C {1:1 atomic ratio} (○) and PtMo/C {5:1 atomic ratio, Pt:Mo} (|). Data for Pt/C with pure H_2 as anode feed is provided for reference (■). PEM operating conditions were 85 °C, 60/50 psig cathode anode backpressure, 100% humidified conditions. The cathode electrode in all cases was 20% Pt/C (0.4 mg cm^{-2}) [ELAT electrode, from De Nora, ETEK division] with oxygen flow.

tion can be made on the basis of the corresponding anode polarization curves (Fig. 2(b)), where a polarization curve in pure H_2 is provided for comparison. Anode polarization of all electrocatalysts reported in this investigation gave very close values for pure H_2, as a result only the plot for Pt/C is used as a representative polarization curve. This lack of variation in the anode polarization with pure H_2 is consistent with previous data [27], which compared the steady-state anode polarization behavior of similar nano-dispersed Pt and alloys of Pt with the first row transition series ranging from Cr to Ni. This is also consistent with our prior report [32] on Pt and PtRu/C (1:1), where similar variations were reported for both these electrocatalysts as a function of temperature in the range 40–115 °C. Detailed analysis of the electrode kinetic data in this

previous study [27], including comparison of the activation energies indicated negligible differences in the activity for hydrogen oxidation as a consequence of alloying. Hence the differences in the single cell polarization is almost entirely due to differences in the electrocatalytic activity for CO oxidation on the different electrocatalyst surfaces as shown in the half-cell polarization data in Fig. 2. Comparison of the single cell performance as well as the anode polarization profiles for the three electrocatalysts under conditions of H_2 [100 ppm CO]/O_2 shows that the PtMo (5:1) maintains superior CO tolerance as compared to PtRu (1:1), both of which are significantly higher than Pt/C. This result is in agreement with those previously reported based on a similar comparison using PtMo (4:1 atomic ratio) [21] and more recently [20] with a comparison of the same three electrocatalysts with the PtMo atomic ratio being 3:1. A more quantitative picture of the comparison shown in Fig. 2(a and b) is delineated in Table 2, where the current densities (after *iR* correction) at two different overpotentials (100 and 50 mV) are listed for the three electrocatalysts, PtRu (1:1), Pt, and PtMo (5:1). As is evident from the values in Table 2, PtMo (5:1), exhibits between 3- and 3.5-fold (depending on the overpotential at which the comparison is made) enhancement in performance as compared to the current state of the art electrocatalyst PtRu (1:1). The corresponding enhancement relative to Pt/C is greater than fourfold.

Also shown in Fig. 2 is a comparison of the polarization profiles for reformate with the composition of 45% H_2, 10 ppm CO, 15% CO_2, 1% CH_4 balance N_2. This comparison, both in terms of single cell (Fig. 2(a)) as well as anode polarization (Fig. 2(b)) shows that the trend in the terms of tolerance to this reformate composition is the same as those observed earlier with H_2 [100 ppm CO] in the anode feed stream. It is important to emphasize that in this case the reformate feed had 10 ppm of CO and 15% (by dry gas volumetric basis) of CO_2. As is evident from the plots, PtMo (5:1) exhibits significantly better reformate tolerance as compared to PtRu (1:1) and Pt/C. Further, the difference in overpotential losses for PtMo (5:1) under both CO [100 ppm] and reformate feed [10 ppm CO and 15 v/o CO_2] are relatively small as compared to Pt and PtRu (1:1). The choice of reformate composition was to assess poisoning due to the reverse shift reaction of CO_2, and probe for any additional poisoning effects CO_2 could contribute. As a result the concentration of CO was kept low at 10 ppm.

Table 2
Electrode kinetic parameters for CO tolerance using H_2 [100 ppm CO]/O_2 feed in a 5 cm^2 MEA, PEM fuel cell operating at 85 °C, 60/50 psig cathode, anode backpressure, 100% humidified conditions

Electrocatalyst	Current density at 100 mV j/mA cm^{-2}	Current density at 50 mV j/mA cm^{-2}
Pt/C	115	75
PtRu/C	150	90
PtMo/C	475	325

Current densities at 100 and 50 mV anode overpotential are compared for Pt/C, PtRu/C (1:1) and PtMo/C (5:1). Atomic composition is expressed as a percent, Pt:M ratio, where M is the alloying element.

This result is in contrast to a recent report, in which a similar comparison is made between Pt, PtRu (1:1) and PtMo (3:1) using 25% CO_2, balance N_2 (dry gas composition) [20]. Here the overpotential loss, compared at 0.5 A cm^{-2} due to the presence of CO_2 for PtRu (1:1) was similar to the effect of Pt with H_2 [10 ppm of CO]. In contrast, the overpotential loss (at the same current density) for PtMo (3:1) was significantly higher, and closer to the effect of Pt with H_2 [100 ppm of CO]. However, the electrocatalysts used in this study had widely fluctuating roughness factors (electrochemically active surface areas determined from hydrogen adsorption region of the cyclic voltammograms), between PtRu and PtMo despite close particle size in terms of their diffracting domains. Therefore a more detailed and systematic evaluation is required, where both the effect of CO tolerance and the reverse shift reaction are examined in detail for the PtMo electrocatalyst.

3.3. The issue of CO tolerance

A more detailed comparison of the anode polarization response can be made more appropriately using the corresponding Tafel response. Such a comparison has been reported earlier by us with PtMo/C (4:1) alloy (same source), PtRu/C (1:1) and Pt/C [33]. Detailed examination of Fig. 2(b) shows that in the absence of CO, both reactions (2) and (3) are very fast (see Section 2), the overall reaction kinetics are described by a very large exchange current density and a Tafel slope (b) close to 30 mV dec^{-1}. On the other hand, in the presence of CO, depending on the extent of CO coverage, reaction (2) may become the rate-determining step. However, at low overpotential or low current densities the surface coverage of H may be enough to allow reaction (3) to occur at full speed, which explains the values of Tafel slopes of 20–30 mV dec^{-1} obtained experimentally for overpotentials less than 50 mV for all catalysts. This has been shown previously [33] and is qualitatively evident from the closeness of the overpotential values at low current densities (below 100 mA cm^{-2}). At higher overpotentials, while the rate of reaction (2) is negligible, the current generation is controlled by the rate of H adsorption, and a limiting current may be observed in the polarization diagram. Under these conditions, the hydrogen current originates only from the oxidation of the M–H being formed on

the holes of a compact CO surface monolayer. As pointed out above, for Pt/C, limiting currents were clearly seen at 85 °C, 100 ppm CO (Fig. 2(b)). The appearance of a limiting current is less evident for PtRu/C and not observed for PtMo/C. The absence of limiting currents can be explained either by a weakening of the CO adsorption process (reaction (2)) and/or to a 'cleaning' of the surface by the CO oxidation step (reaction (3)). Prior reaction kinetic modeling efforts, comparing PtRu/C (1:1) and Pt/C, with PtMo/C (4:1) [33] and PtSn/C (3:1) [34], have shown that CO oxidation is the most important contributor to the polarization response in the case of CO tolerance (in the presence of H_2+CO mixtures). The fact that PtMo/C (5:1) shows very good CO tolerance implies that the Mo oxy-hydroxides are very well dispersed on the PtMo alloy nanocluster surface.

Fig. 3(a) shows both the single cell and the anode polarization plot for PtMo/C as a function of alloying composition. The experimental conditions were 70 °C (cell temperature), 100% relative humidity, 16/11 psig (anode and cathode backpressure) and H_2 [50 ppm CO]/O_2 feed in a cell with a 5 cm^2 MEA. The results in Fig. 3(a) show minimal effect of change of alloying composition in the range 1:1 to 5:1 (Pt:Mo), as is evident from the closeness of both the single cell and anode polarization profiles. This result is somewhat different from those reported earlier by Grgur et al. [22], where a composition containing 23 a/o Mo was found to be optimal for CO oxidation. However these results were obtained with well defined bulk surface compositions, comparative analysis with corresponding compositions in supported nano-cluster alloys of PtMo did not provide the same result. [22] A qualitative explanation based on the possibility of surface segregation was used as an argument to explain the differences in the results with bulk and supported electrocatalysts. Our results shown in Fig. 3(a) provide a wider range of alloying compositions as well as better characterization of the electrocatalysts in terms of nano-cluster composition (atomic ratio), and particle size.

Fig. 3(b) shows the corresponding cyclic voltammograms with and without the presence of 50 ppm of CO in the H_2 feed. These experiments, which were carried out in a PEM single cell with built in RHE reference electrode, involved purging the working electrode (anode electrode of the MEA) with H_2 with or without 50 ppm CO for at least 1 h. The cyclic voltammograms were taken in the PEM single cell assembly with the working electrode under N_2 purge (after at least a one-hour purge with N_2) and the reference and counter electrode with H_2 purge, under conditions of 100% relative humidity and 50 °C cell temperature. The cyclic voltammograms in the absence of CO show several interesting features, details of which have been discussed previously [21,28]. Briefly, the cyclic voltammograms

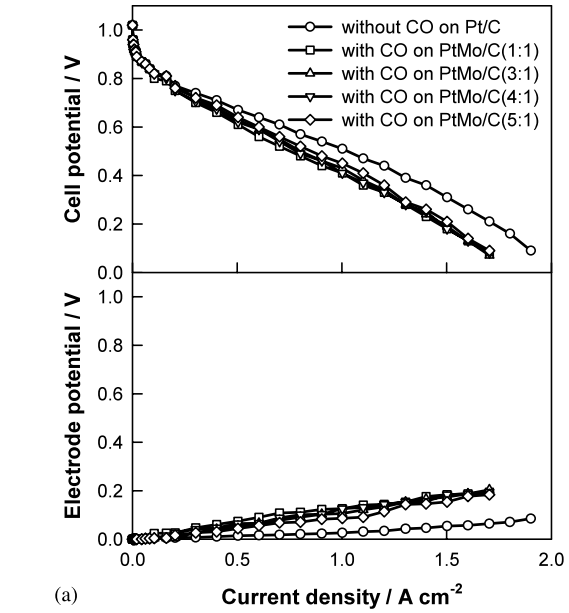

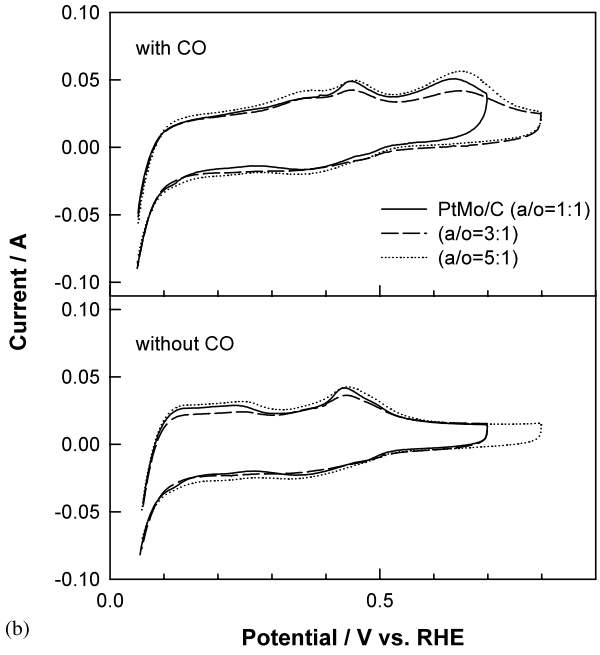

Fig. 3. (a) Steady-state single and half cell polarization measurements with an anode feed of H_2 [50 ppm CO] for PtMo electrocatalysts as a function of different Pt:Mo atomic ratios (1:1, □; 3:1, △; 4:1, ▽; and 5:1, ◇). Data for a Pt/C electrode with pure H_2 (○) anode feed is included as a reference. PEM operating conditions were 70 °C, 16/11 psig anode, cathode backpressure respectively. The cathode electrode in all cases was 20% Pt/C (0.4 mg cm^{-2}) [ELAT electrode, from De Nora, ETEK division] with oxygen flow. (b) Cyclic voltammograms for PtMo electrocatalysts with varying atomic ratios (1:1, —; 3:1,-- -; and 5:1, ···) with and without H_2 [100 ppm CO] purge (at least 1 h), followed by 1 h N_2 feed. Cyclic voltammograms were recorded with the anode working electrode under N_2 flow, 100% humidification conditions and the cathode counter/reference under H_2 flow, 100% humidification.

show evidence of both Pt and Mo features although the Pt–H_{upd} region is not as defined as the Pt/C or PtRu/C

electrodes. As in the case of the bulk alloy [22], the voltammogram of PtMo/C in the absence of CO shows redox behavior in the potential range of 0.43–0.50 V versus RHE which can be attributed to Mo. Comparison with the Pourbaix diagram for Mo indicates that this redox behavior is most likely due to a $Mo^{4+} \leftrightarrow Mo^{6+}$ oxidation state change. A recent report by us [28], using in situ XANES spectroscopy at the Mo K edge for these electrocatalysts has shown this oxidation state change to be $Mo^{5+} \leftrightarrow Mo^{6+}$. Repeated cycling between 0.05 and 1.2 V for 50 cycles showed no changes indicating minimal dissolution of Mo from these electrocatalysts. The similarity of anode polarization behavior exhibited by PtMo as a function of variation in alloy composition indicates that a very small amount of Mo is required for CO tolerance. The discussion related to the anode polarization characteristics of Pt, PtRu (1:1) and PtMo (5:1) shown in Fig. 2(b) implies an efficient formation of gaps in the compact CO adsorbed layer enabling sufficient hydrogen oxidation kinetics to occur and thereby avoiding any limiting behavior. This invariance with alloying composition in the range 1:1 to 5:1 shows that (a) Mo oxy-hydroxides are very efficient in electro-oxidation of CO, which as shown in the subsequent discussions below is initiated at low potentials (close to hydrogen evolution potentials). (b) These Mo species are well dispersed on the electrocatalyst surface to enable the formation of gaps in the compact CO adsorbed layer and hence enable hydrogen oxidation. Earlier reports on PtRu show that, in contrast to PtMo, there is a variation on anode polarization as a function of alloying composition (atomic ratio), with PtRu (1:1) being optimal [35].

Experiments with H_2 [50 ppm CO] purge for 1 h followed by a minimum of 1 h of N_2 purge under the same PEM single cell conditions delineated above (Fig. 3(b)) indicates that both Pt and Mo are active for the CO oxidation. CO oxidation is first initiated at lower potentials by oxygenated species on the Mo surface at ca. 0.05 V. The second peak at approximately 0.65 V has been shown to be due to CO oxidation by oxides of Pt. This has been reported recently by us using both a comparison with the corresponding voltammogram for Pt/C as well as with in situ XAS at the Pt edge (see Ref. [28] for details). Prior studies [36] with bulk PtMo (3:1) in 2% CO in Ar have shown CO oxidation to occur at potentials as low as 0.05 V vs. RHE at 60 °C. This prior study suggested that the primary role of Mo was to create holes in the compact CO adsorbed layer by initiating its oxidation at such low potentials. The presence of two distinct peaks is significant, in that it is in complete contrast to the corresponding voltammetric response from electrocatalysts such as PtRu/C and PtSn/C. This indicates a unique role for Mo in these electrocatalysts because it exhibits a more complex behavior as compared to predictions based on the 'bifunctional mechanism', where the oxides on the more oxidizable element provide the necessary oxygenated species for the CO oxidation on Pt. It is interesting to note that the description of features mentioned above both with and without the presence of CO in H_2 over the working electrode, are the same for all the alloying compositions in the range 1:1 to 5:1. This is important, since even with a 5:1 composition, there is a sufficient amount of dispersed Mo on the surface of the electrocatalyst to provide for the Mo features described above.

Fig. 4(a) shows the anode polarization profiles for Pt, PtRu (1:1) and PtMo (5:1) as a function of varying amounts of CO in H_2 in the range of 5–100 ppm. The data shown are for an 85 °C cell temperature under 100% humidification and 60/50 psig backpressure (cathode and anode electrodes, respectively). As evident from the data, the variation of anode polarization is the highest in the case of Pt, followed by PtRu (1:1) and finally PtMo (5:1), where the variation as a function of CO concentration (in the range 5 to 100 ppm) is minimal. Experiments using PtMo (3:1 and 1:1 a/o) also gave similar results, with minimal variation of anode polarization within the CO concentration range of 5–100 ppm. Detailed evaluation of the results published recently by Ball et al. [20], shows similar behavior, where PtMo(3:1), showed the lowest variation in overpotential loss at 0.5 A cm^{-2} when the anode gas composition was changed from H_2 [CO 10 to 100 ppm]. A log–log plot of current density at 70 mV (*IR* corrected data) versus CO concentration is plotted in Fig. 4(b). As is evident from the plot, all three electrocatalysts exhibit strong negative slopes and, hence, reaction orders. The reaction orders for Pt and PtMo (5:1) were −0.4 and −0.36, respectively, while the value for PtRu (1:1) was −0.48. Within the limits of error inherent in these measurements (typically 15–20% variation based on four sets of experiments), all the reaction orders are approximately −1/2. These negative reaction orders are consistent with our previous results [32] and others, such as those on PtRu (bulk alloys), where prior results at 0.4 V have shown a similar negative reaction order. Details of the significance of this negative reaction order and its implications in terms of the CO tolerance mechanism on these different alloy electrocatalysts is the subject of a separate report currently under preparation.

Fig. 4(c) shows the plot of CO coverage calculated according to methodology described briefly in Section 2 versus the Ln([CO]/[H_2]) for all three catalysts. A straight line for this plot represents Temkin behavior as described in more detail previously [37]. Superimposed on this plot of variation of CO content in the H_2 stream is the calculated coverage of CO from a reformate feed. The reformate composition in this case is the same as described earlier (45% H_2, 10 ppm CO, 15% CO_2, 1% CH_4 balanced with N_2). The super-

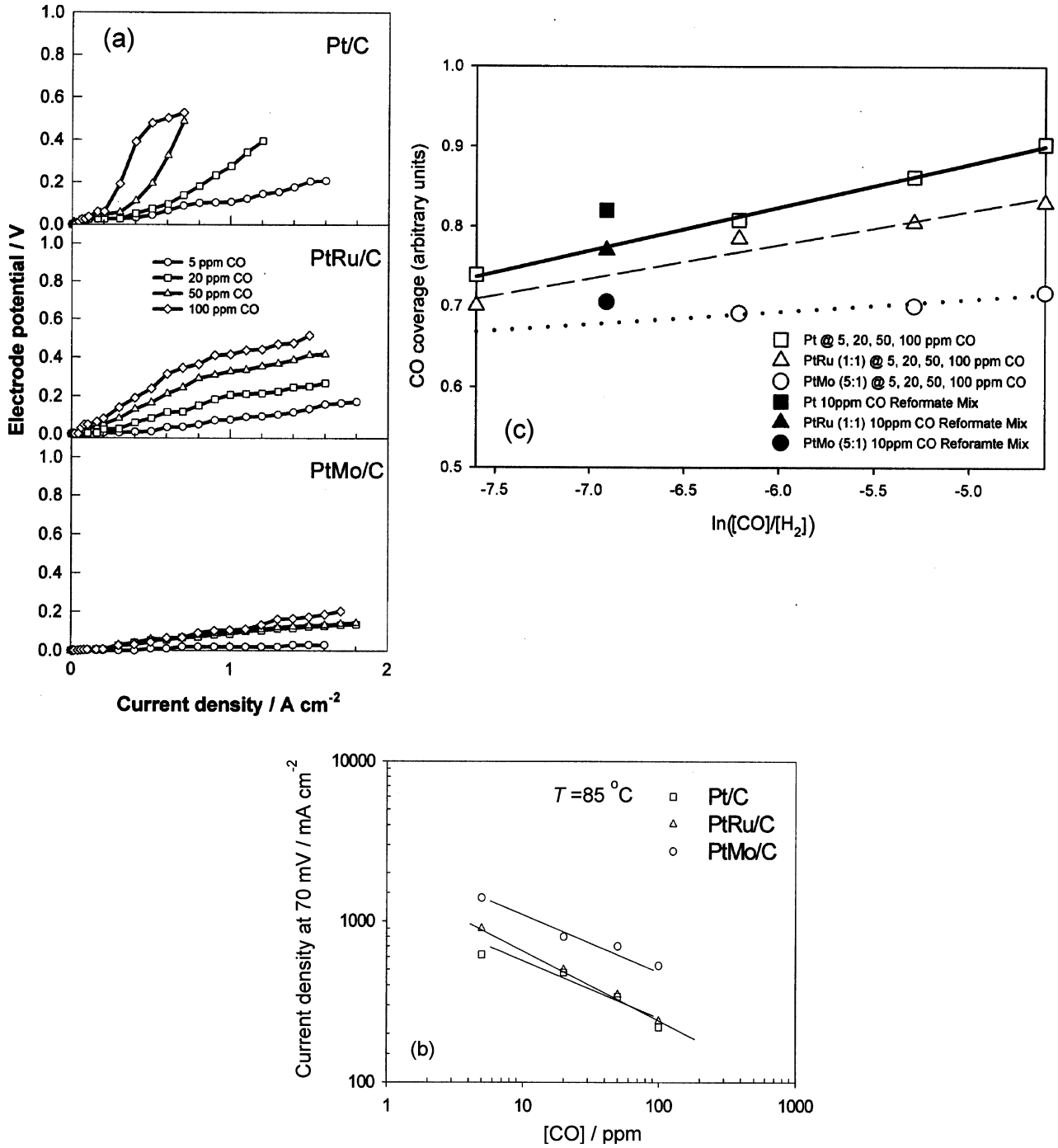

Fig. 4. (a) Steady-state anode polarization for Pt/C, PtRu (1:1, atomic ratio) and PtMo/C (5;1 atomic ratio, Pt:Mo) as a function of different CO content in the H_2 feed. H_2 [5 ppm CO, (○); 20 ppm CO, (□); 50 ppm CO (△) and 100 ppm CO (◇)]. (b) Log–log plot of CO concentration and current density at 70 mV for Pt, PtRu (1:1) and PtMo (5:1) and (c) Plot of Ln [CO]/[H_2] vs. CO coverage (θ) for Pt/C (□), PtRu (1:1, atomic ratio, △) and PtMo/C (5;1 atomic ratio, Pt:Mo, ○). Coverage data is also plotted for 10 ppm CO + reformate mixture (corresponding filled symbols). PEM operating conditions for these tests were 85 °C, 60/50 cathode, anode backpressure, 100% humidification condition, with O_2 as the cathode gas feed. The cathode electrode in all cases was 20% Pt/C (0.4 mg cm^{-2}) [ELAT electrode, from De Nora, ETEK division].

imposed value based on the CO content of 10 ppm in the reformate (Ln [CO]/[H_2]) shows additional coverage due to the presence of CO_2. This is represented as a positive shift in the CO coverage above the isotherm of each of the electrocatalysts. This clearly demonstrates that CO_2 has an additive poisoning effect. The next section

examines in more detail this additional poisoning due to the reverse shift reaction and its implication on PtRu and PtMo alloy electrocatalysts.

3.4. Effect of CO_2 in reformate feed

3.4.1. Results of dynamic tests using cyclic voltammetry

In order to understand the effect of CO_2 in reformate feed and its potential poisoning effect due to the reverse shift type reaction (formation of CO), a systematic study was conducted with various CO_2/H_2 mixtures. Fig. 5, shows a set of cyclic voltammograms conducted in a PEM fuel cell after a series of polarization measurements with varying H_2/CO_2 ratios (in the range of 40:60 to 60:40 mole ratio) and after similar measurements with H_2 [100 ppm CO]. In the case of experiments with varying H_2/CO_2 molar ratios, the final polarization measurement was conducted with a 40:60 mole ratio of H_2:CO_2. The cyclic voltammograms were run under a N_2 flow on the working electrode (anode), after purging for at least 1 h, with the counter and reference electrodes remaining under a pure H_2 feed. The PEM fuel cell for all of the cyclic voltammograms in Fig. 5 were kept under the same conditions as the last polarization measurement, 85 °C cell temperature, 100% humidification and 60/50 psig backpressure for the cathode and anode electrode respectively. Comparison of the results with H_2/CO_2 (40:60 mole ratio) and those after H_2 [100 ppm CO] purge show qualitatively the same CO stripping peaks, thereby unequivocally showing that CO_2 purged in the presence of H_2 results in CO poisoning of Pt and the Pt alloy electrocatalysts (both PtRu and PtMo). The comparison of the stripping peaks shows a perfect match in terms of peak positions. This congruence of CO stripping peak positions are in agreement with prior reports [8,38–40]; however, a recent report [41] has shown the stripping peak due to reduced CO_2 to be initiated earlier than the corresponding stripping peak for pre-adsorbed CO. Prior reports comparing stripping peaks of reduced CO_2 and pre-adsorbed CO have shown the influence of strongly and weakly adsorbed CO, which manifests itself as two stripping peaks. This was not observed in our experiments, though the existence of overlapping peaks in the voltammograms shown in Figs. 5 and 6 cannot be ruled out, especially for Pt/C. A qualitative comparison of the difference in the charge for CO stripping between H_2 [100 ppm CO] and H_2/CO_2 (40;60 mole ratio) shows close congruence in the case of Pt, followed by PtMo (5:1) and PtRu (1:1). These correspond qualitatively to the level of poisoning due to reduced CO_2 in these various electrocatalysts. In the case of a purge with a 60:40 mole ratio of H_2/CO_2, the level of poisoning on Pt appears to be close to the effect with 100 ppm of CO, a somewhat lower level of poisoning is apparent with PtMo (5:1). For PtRu (1:1), the corresponding difference was much larger as compared to Pt and PtMo (5:1), thereby indicating a significantly lower level of poisoning due to the presence of CO_2 (60% mole ratio in H_2). Accurate comparison of the coverage by CO type

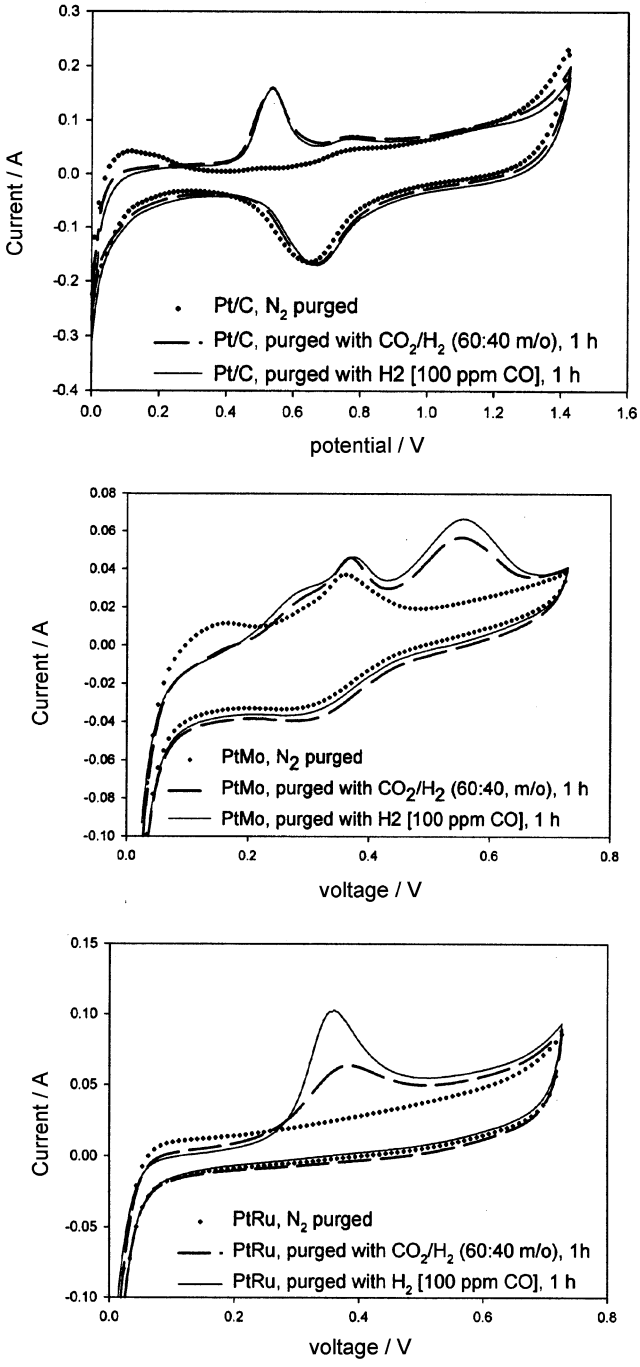

Fig. 5. Cyclic voltammograms for (a) Pt, (b) PtRu (1:1 atomic ratio) and (c) PtMo (5:1 atomic ratio, Pt:Mo) as a function of different anode gas feeds. H_2 purge (·), CO_2/H_2 (60:40 m/o) (---) and H_2 (100 ppm CO) (—). PEM operating conditions for these tests were 85 °C, 60/50 cathode, anode backpressure, 100% humidification condition, with N_2 gas feed on the working electrode during cyclic voltammetry (at least 1 h purge). The cathode electrode in all cases was 20% Pt/C (0.4 mg cm^{-2}) [ELAT electrode, from De Nora, ETEK division] with hydrogen flow.

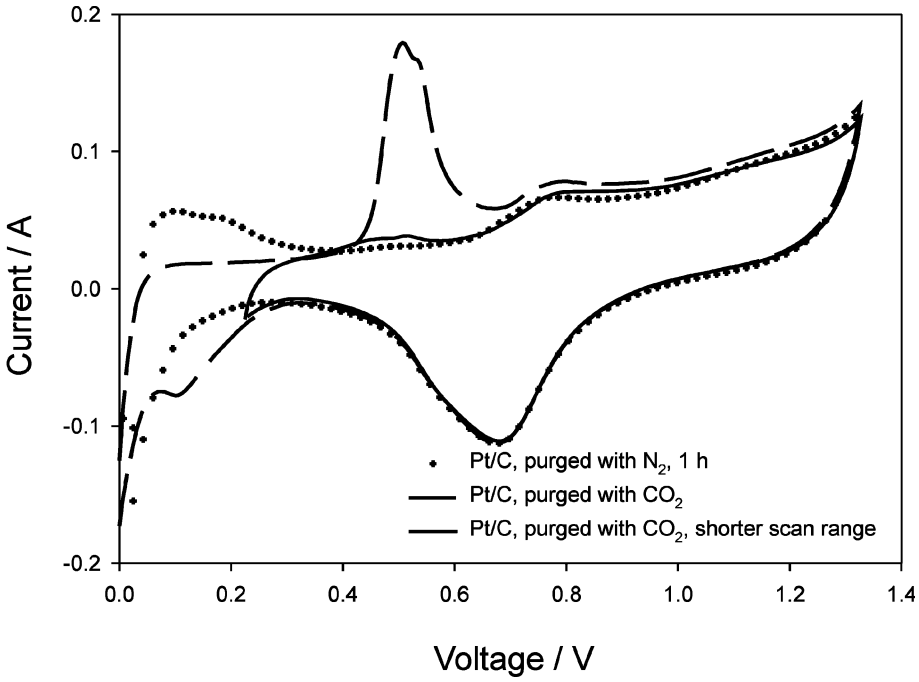

Fig. 6. Representative plot showing the cyclic voltammograms for Pt/C under conditions of flowing pure CO_2 over the anode working electrode. Cathode under pure H_2. PEM operating conditions: 85 °C, 60/50 cathode and anode backpressure respectively, 100% humidification conditions and the cathode electrode under pure H_2 flow. Data for Pt/C under N_2 flow is included for reference.

species as a result of a CO_2/H_2 purge is difficult due to the dynamic conditions of cyclic voltammetry, which does not offer adequate correction for contributions due to diffusion and interfacial capacitance in a typical PEM gas diffusion electrode configuration. In a qualitative sense, these results are in agreement with a recently published report [41], where a comparison was made between the extent of coverage between Pt/C and PtRu/C (from ETEK div., of De Nora). In this prior study [41] the relative peak height contribution of cyclic voltammograms showed a value of $\theta_{\text{reduced } CO_2}$ of 0.78, for Pt/C, compared to 0.15 for PtRu/C. This study also pointed out some of the difficulties in using cyclic voltammetry as a tool for determining surface coverage. Here the quantitative charges for surface desorption are more ambiguous. Use of such analysis for PtMo/C is more difficult due to the presence of an oxidative peak at $\sim$ 0.45 V versus RHE [28]. As reported previously [28], this is part of a redox couple involving $Mo^{+5} \leftrightarrow Mo^{+6}$.

In order to corroborate the results in Fig. 5 further, a set of cyclic voltammograms was run in a PEM fuel cell with pure CO_2 flowing on the working electrode (anode electrode), with pure H_2 flow on the counter and the reference electrodes. Fig. 6 is a representative cyclic voltammogram for Pt/C, which shows the characteristic peak for CO stripping when the scan is run between potentials of 0.025 and 1.3 V versus RHE. Truncation of the same scan with flowing CO_2, between potentials of 0.225 and 1.3 V, results in the elimination of the CO stripping peak, thereby showing that the presence of adsorbed hydrogen on the Pt surface is essential for the reverse shift reaction. It also confirms the absence of any CO impurity in the CO_2 gas used. Both the PtRu/C (1:1) and the PtMo/C (5:1, as well as the other alloying compositions) gave the same result as those shown with Pt/C (Fig. 6). This cyclic voltammogram is in agreement with a recent report [41], where a cyclic voltammetric comparison was made to investigate the effect of CO_2 in poisoning the anode electrode comparing behavior with PtRu (1:1) and Pt/C. Here, the electrode was pre-polarized at several different potentials, during CO_2 purge in 1 M H_2SO_4. Cyclic voltammograms conducted under N_2 flow, following such a purge showed that a shift away from the hydrogen adsorption, evolution and desorption regions (anodic and cathodic branches of the hydrogen region) into the double layer region results in the elimination of the CO stripping peak, thus leading to a similar conclusion as that obtained from Fig. 6. In our case the experiments were conducted under flowing CO_2 conditions in an actual PEM fuel cell operating at 85 °C, 60/50 psig (backpressure, cathode/anode electrode respectively), 100% humidification.

3.4.2. Results of steady-state polarization using PEM single and half cell data

For a more systematic understanding of the effect of CO_2 as a surface poison and its interaction with the Pt and Pt alloy electrocatalyst surface, several steady-state polarization tests were run as a function of the CO_2:H_2 mole ratio (in the range 40:60 to 60:40), without the

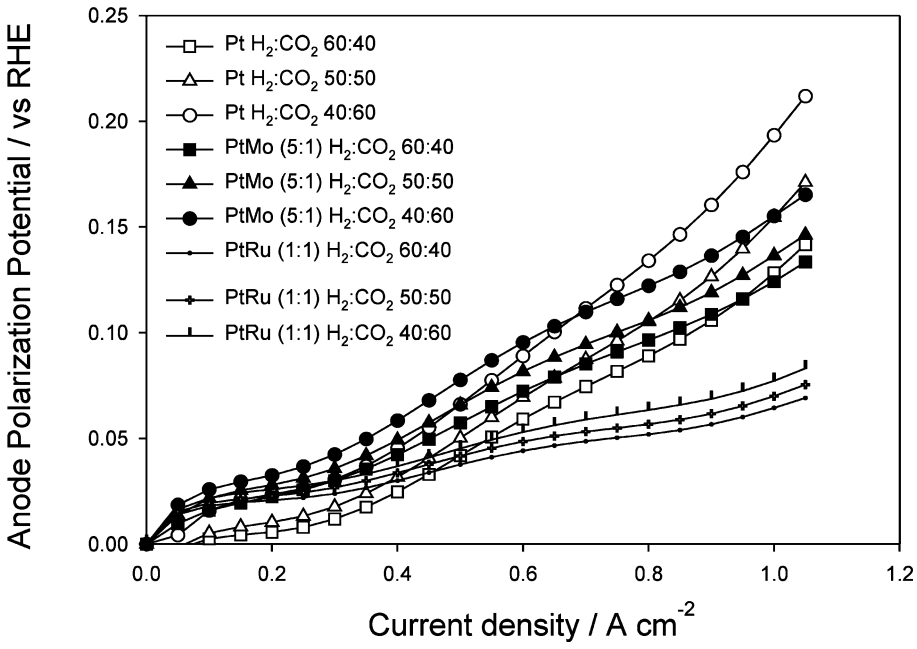

Fig. 7. Steady-state half cell anode polarization profile as a function of different CO_2:H_2 ratios for Pt/C, 60:40 (□), 50:50 (△) and 40:60 (○), PtMo/C (5:1 atomic ratio, Pt:Mo), 60:40 (■), 50:50 (▲) and 40:60 (●) and PtRu/C (1:1 atomic ratio, Pt:Ru), 60:40 (·), 50:50 (✚) and 40:60 (▮). PEM operating conditions for these tests were 85 °C, 60/50 cathode, anode backpressure, 100% humidification condition, with O_2 as the cathode gas feed. The cathode electrode in all cases was 20% Pt/C (0.4 mg cm^{-2}) [ELAT electrode, from De Nora, ETEK division] with oxygen flow.

presence of CO. The results of these tests in terms of anode polarization at 85 °C, 100% humidification, 60/50 psig (cathode anode backpressure, respectively) are given in Fig. 7. This figure compares the anode polarization curves for PtRu (1:1), Pt and PtMo (5:1) at three different H_2:CO_2 ratios (40:60, 50:50 and 60:40 mol%). A comparison of these polarization profiles shows that, for an increase of partial pressure of CO_2, there is an increase in the overpotential loss. The extent of this increase is lowest for PtRu (1:1) in comparison to PtMo (5:1) and Pt. Both Pt and PtMo (5:1) show similar behavior in overpotential losses above 0.4 A cm^{-2} current density. This current density serves as an approximate dividing line between the behavior exhibited by the alloy electrocatalysts (PtRu and PtMo) and Pt. Below this current density, the anode polarization profiles for alloys show close similarity and exhibit slightly higher losses as compared to Pt for CO_2:H_2 ratios up to 50:50. A higher CO_2:H_2 ratio (60:40) shows no difference with the alloy electrocatalysts. Above 0.4 A cm^{-2}, the PtRu (1:1) shows a significantly lower overpotential loss as compared to Pt and PtMo (5:1). Further, the increase in overpotential losses as a function of CO_2 partial pressure was significantly lower than those for Pt and PtMo (5:1), through the entire current density range. Both Pt and PtMo (5:1) showed very similar variation of overpotential losses as a function of increase in CO_2 partial pressure.

A more quantitative depiction of the overpotential loss, $\Delta V_{\text{poisoning}}$, as a function of partial pressure of CO_2 ($\ln p_{CO_2}$), is shown in Fig. 8. All comparisons shown in this figure are from corresponding *i*R corrected anode polarization profiles. Also shown in this figure is the *iR* corrected data for the dilution effect (solid line) and the corresponding data points for H_2:N_2 (same variation in molar ratio as H_2:CO_2). There is no significant effect of increase of current density as a function of dilution (within the same experimental limits). All overpotential losses shown in Fig. 8, are therefore corrected for this dilution effect and therefore exclusively reflect the overpotential loss due to poisoning.

At lower current density (0.25 A cm^{-2}), Pt shows overpotential losses which are very close to that due to dilution up to CO_2 partial pressure corresponding to a mole ratio of 50:50, beyond which there is a very small deviation (corresponding to a 60:40 mole ratio of H_2:CO_2). The overpotential losses increase dramatically at and beyond 0.5 A cm^{-2} for Pt, with the slope of the increase in overpotential losses changing significantly when transitioning from 50:50 to 60:40 mole ratio of CO_2:H_2. PtRu (1:1) and PtMo (5:1) show a similar, albeit a somewhat larger overpotential loss as compared to Pt at lower current density (0.25 A cm^{-2}). The behavior of the two alloys is very similar in this low current density regime, through the entire experimental range of CO_2 partial pressures. At higher current density, PtRu shows the lowest variation (dotted lines in Fig. 8) of overpotential loss as a function of both increasing current density (in the range of 0.5–1 A cm^{-2}) and as a function of increasing partial pressure of CO_2.

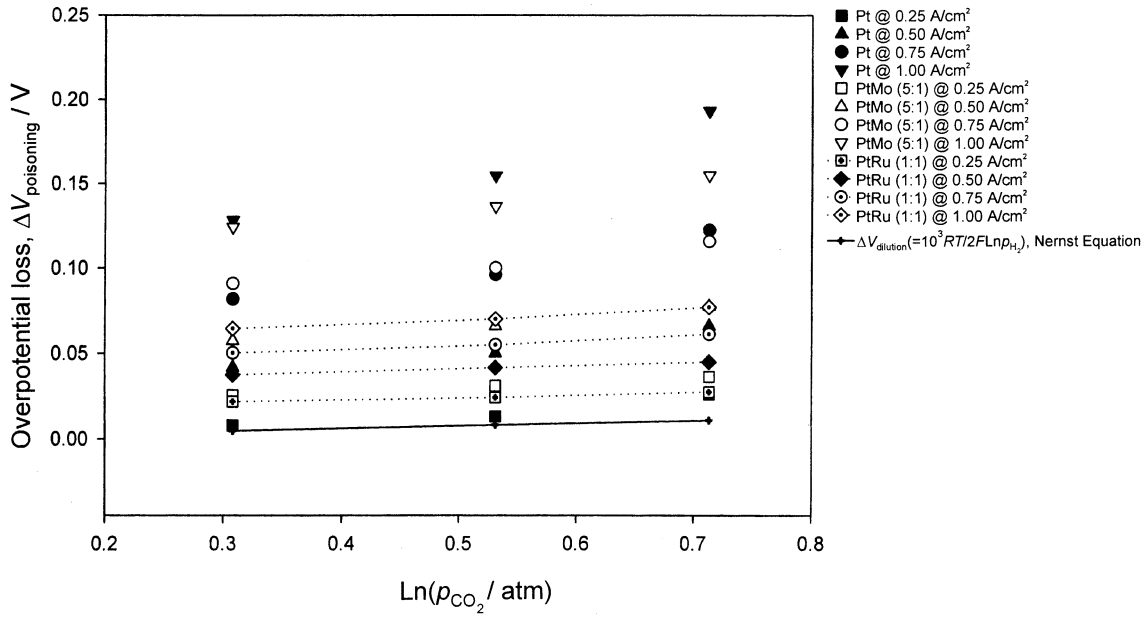

Fig. 8. Plot of overpotential loss (ΔV_{pois}) vs. Ln p_{CO_2} at different current densities. Pt/C [0.25 A cm^{-2} (■), 0.5 A cm^{-2} (▲), 0.75 A cm^{-2} (●) and 1 A cm^{-2} (▼)], PtMo/C (5:1 atomic ratio, Pt:Mo) [0.25 A cm^{-2} (□), 0.5 A cm^{-2} (△), 0.75 A cm^{-2} (○) and 1 A cm^{-2} (▽)] and PtRu/C (1:1 atomic ratio, Pt:Ru) [0.25 A cm^{-2} (⊡), 0.5 A cm^{-2} (◆), 0.75 (◉) and 1 A cm^{-2} (◈)]. Voltage loss due to dilution is also plotted as a reference, data (✚) and theoretical line (—) based on the Nernst equation. Note that the dashed lines show the overpotential losses for PtRu/C at various current densities.

Comparison of Pt and PtMo (5:1) above 0.5 A cm^{-2} current density shows a similar variation in overpotential loss as a function of increasing partial pressure of CO_2. However the overpotential losses start to deviate sharply at higher CO_2 partial pressure with Pt showing higher deviations than PtMo, especially at partial pressures corresponding to 60:40 CO_2:H_2. The deviation between Pt and PtMo overpotentials is most pronounced at high current densities (1 A cm^{-2}) at the highest CO_2 partial pressure.

Figs. 7 and 8, provide a comparison of overpotential losses for PtMo (5:1) with PtRu (1:1), where PtRu exhibits significantly lower overpotential losses beyond a current density of 0.25 A cm^{-2}, especially at higher partial pressures of CO_2 corresponding to a mole ratio of 60: 40 CO_2: H_2. This trend is in agreement with results published earlier by Ball et al. [20], where a comparison of PtRu (1:1) is made with PtMo (3:1) with a H_2:CO_2 molar ratio of (75:25). In this prior report, negligible overpotential loss is reported for PtRu (1:1) in contrast to PtMo (3:1), wherein an overpotential loss of approximately 0.25 V is reported. This result for PtMo is very different from ours and can be attributed only to the different method of electrocatalyst preparation used.

Fig. 9 shows the corresponding effect on the overpotential for hydrogen oxidation as a function of partial pressure of CO_2 for three different alloying compositions of PtMo (1:1, 3:1 and 5:1). The corresponding value for PtRu (1:1) is also shown for comparison. As is evident from this figure, at low current density (0.25 A cm^{-2}) all alloying compositions of PtMo exhibit similar losses. However, for higher current density, such as 0.5 A cm^{-2}, the alloying composition appears to play a very important role in determining the extent of overpotential loss. The most striking effect of this is the close correspondence of the hydrogen overpotential losses for the alloying composition 1:1, wherein both PtRu and PtMo exhibit similar overpotential losses. This clearly points to the availability of Pt sites as the most important parameter determining the extent of hydrogen overpotential losses due to formation of reduced CO_2 species. This is clearly in contrast to the results with CO tolerance, where the effect of variation of alloying composition had a negligible effect on the anode polarization. As expected therefore, the largest deviations in the hydrogen overpotential loss for the different alloying compositions of PtMo primarily occur at the higher current density (1 A cm^{-2}) and partial pressure of CO_2.

All these results clearly point to the importance of the available Pt surface as the prime factor in determining the extent of anode overpotential loss due to reduced CO_2. This has been described as the 'ensemble effect' in earlier publications such as those by Arvia and coworkers [42–44], where the 'ensemble' is the number and shape of contiguous empty sites necessary for chemisorption of a particular molecule. In the context of this present work it refers to the need for both hydrogen and CO_2 molecules to have the appropriate adsorption geometry to enable formation of reduced CO_2. Hence, on the Pt surface there is a competition between hydrogen oxidation and the formation of reduced CO_2

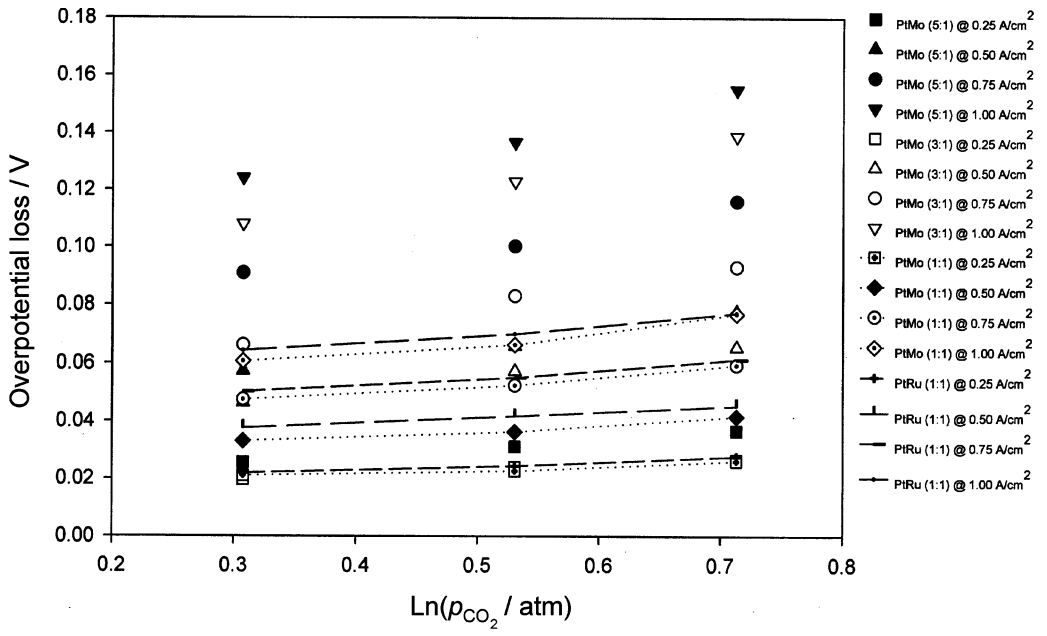

Fig. 9. Plot of overpotential loss of (ΔV_{pois}) vs. Ln p_{CO_2} at different current densities for various PtMo alloying compositions. PtMo (5:1 atomic ratio, Pt:Mo) [C [0.25 A cm^{-2} (■), 0.5 A cm^{-2} (▲), 0.75 A cm^{-2} (●) and 1 A cm^{-2} (▼)], PtMo (3:1 atomic ratio, Pt:Mo) [0.25 A cm^{-2} (□), 0.5 A cm^{-2} (△), 0.75 A cm^{-2} (○) and 1 A cm^{-2} (▽)] and PtMo (1:1 atomic ratio, Pt:Mo) [0.25 A cm^{-2} (⊡), 0.5 A cm^{-2} (◆), 0.75 (⊙) and 1 A cm^{-2} (◈)]. Data for PtRu (1:1 atomic ratio, Pt:Ru) [0.25 A cm^{-2} (╋),0.5 A cm^{-2} (▮), 0.75 (▬) and 1 A cm^{-2} (·). The dotted and dashed lines link the overpotential losses for PtMo/C (1:1) and PtRu/C (1:1 atomic ratio) at various current densities.

species. For CO tolerance, CO displaces surface hydrogen to form compact islands. Formation of holes in these compact islands to enable sufficient hydrogen oxidation to occur happens only when initiated at the edge of these islands by the anodic activation of water either on Pt (which happens only at potentials higher than 0.65 V) or at more negative potentials on the more oxidizable alloying element Mo or Ru. As a result the dispersion of the more oxidizable Ru and Mo with their corresponding surface oxy-hydroxides on the alloy nanocluster is more important than a simple correlation with alloying composition.

A more detailed examination of the anode polarization profiles in Fig. 7, and the comparison of the anode overpotential loss at low and high current density for Pt and Pt alloys (Figs. 8 and 9) indicate that in the case of alloys, the formation of reduced CO_2 is immediately apparent, even at very low current densities. In contrast, for Pt, such a poisoning effect starts at higher current density, closer to 0.4 A cm^{-2}, up to a partial pressure of CO_2 corresponding to a 50:50 H_2: CO_2 mole ratio. Since in the lower current density range (below 0.25 A cm^{-2}), the effect of the available Pt surface is not expected to make a substantial difference between an alloy such as PtMo (5:1) and Pt, the influence of other parameters such as the surface electron density and the interplay between surface bonded reduced CO_2 species and oxy-hydroxides of Mo and Ru cannot be ruled out.

3.4.3. Discussions

Prior sudies by Arvia and coworkers [42–44] on electro-oxidation of 'reduced CO_2' on electrodispersed Pt electrodes have reported a complex pathway involving the existence of two types of reduced CO_2 species, obeying a Temkin isotherm. They reported first order kinetics at full coverage. Subsequent to formation of free Pt sites, second order kinetics were reported, each proceeding with one of the two types of reduced CO_2 species. These two types of reduced CO_2 species were suggested to be different forms of a CO_2–H_2O clathrate-type structure, depending whether the reaction proceeds via weakly or strongly bonded hydrogen. An apparent activation energy of 80 ± 15 kJ mol^{-1} was reported.

For electro-oxidation of reduced CO_2 species, the Pt surface appears to be the key reaction site. While there are no systematic studies on the formation and electro-reduction of reduced CO_2 on alloying elements such as Ru and Mo, there is a preponderance of evidence suggesting their role to be negligible compared to Pt. A prior report [45] comparing the CO selectivity in the electroreduction of CO_2 on a wide variety of metal electrodes in aqueous electrolytes have shown that a correlation of potential for CO_2 reduction and hydrogen evolution is lowest for Pt in a comparison with a wide selection of metals including several transition elements.

When comparing the behavior of Pt with alloys such as PtRu and PtMo, there are significant differences; these have been elaborated in detail in the discussions of

Figs. 8 and 9. As mentioned above, factors related to the different surface electron density of Pt in the alloy versus unalloyed Pt as well as the interaction of the reduced CO_2 species with the oxy-hydroxides of the alloying element cannot be ruled out. A prior report [46] on electro-oxidation of reduced CO_2 on series of Pt single crystal electrodes strongly support the argument for the difference arising as a result of variation in surface electron density. In this report, a series of single crystal surfaces with various degree of step sites on (111) and (100) surfaces was studied. The activity was directly related to the degree of roughness brought about by introduction of steps and the electrocatalytic activity for CO_2 reduction was directly related to the step atom density. This study suggests that the higher degree of imbalance in the surface electron density (lower d-band vacancy or work function) at the lower coordination step sites enhances the CO_2 electroreduction. A prior report [45] shows that there are three primary modes of CO_2 interaction with the transition elements. In all these, bonding occurs via electron transfer from CO_2 to unoccupied metal orbitals (donation) and backbonding from occupied metal orbitals to the lowest unfilled orbital of CO_2. Most of the prior molecular orbital studies on these types of systems (see Ref. [45] for a review) show that the coordinate bond is mostly stabilized by back-donation from d-orbitals of the metal atom to the anti-bonding π^* orbital of CO_2 rather than by donation from CO_2 to the metal orbitals. Among the most favored coordination geometry is the C-coordination [45], wherein the extra negative charge on the oxygen atom facilitates the protonation to the coordinated CO_2. Interaction with surface adsorbed hydrogen atoms therefore has the potential for producing a wide variety of species including clathrate compounds. The choice of coordination, such as C-coordination has the potential of exhibiting strong dependence on the surface electronic properties of Pt. Prior studies using in situ X-ray absorption spectroscopy have shown very different Pt d-orbital vacancies for PtRu as compared to Pt and a more systematic study of this parameter and the interaction of the oxy-hydroxide species in the electro-oxidation of the reduced CO_2 species is the subject of the second part of this publication.

4. Conclusions

This paper forms the first of a series, examining the anode overpotential loss for PtMo electrocatalysts in the presence of different reformate compositions. The focus here is to understand the overall overpotential loss under typical PEM fuel cell operating conditions in the context of varying amounts of CO_2 in the reformate feed. A series of PtMo electrocatalysts have been evaluated with systematic variation of the Pt:Mo atomic ratio (in the range 1:1 to 5:1). For a better insight into the anode polarization losses, both CO and CO_2 poisoning effects have been examined systematically. This has been presented in the context of both PtRu (1:1) (a current state of the art reformate tolerant electrocatalyst) and Pt.

Evaluation of anode polarization in the context of CO tolerance [H_2 (100 ppm CO)] using varying Pt: Mo atomic ratios (in the range of 1:1 to 5:1) show negligible effects. PtMo exhibits greater than threefold enhancement in CO tolerance as compared to PtRu (1:1) and greater than fourfold enhancement relative to Pt. This is based on current densities at two different overpotentials (50 and 100 mV). The effect of variation of CO content in H_2 (in the range 5 to 100 ppm) also shows the lowest variation in overpotential losses for PtMo electrocatalyst (5:1) followed by PtRu (1:1) and Pt. Correlation of these results on PtMo with the corresponding cyclic voltammetry shows that unlike PtRu, the oxidation of CO on Pt starts at very low potentials on PtMo, thus creating enough holes in the compact CO adlayers to allow efficient oxidation of hydrogen to proceed. The insensitivity of the anode polarization losses with respect to both alloying compositions and the variations of CO content in H_2, shows that the Mo oxy-hydroxides are well dispersed on the PtMo nanoclusters. Subsequently, these act as efficient reaction centers for water activation and hence initiation of holes in the compact CO adsorbed layers.

Comparison of the anode polarization profiles (and corresponding overpotential losses) for PtMo (5:1), PtRu (1:1) and Pt as a function of p_{CO_2} shows that above 0.5 A cm^{-2} current density, Pt and PtMo (5:1) exhibit comparatively closer characteristics in contrast to PtRu (1:1). For PtRu (1:1), results above 0.5 A cm^{-2}, show significantly smaller variation in overpotential losses both in terms of increasing current density and p_{CO_2}. Below 0.5 A cm^{-2}, Pt showed lower overpotential losses as compared to the alloys (both PtRu and PtMo), especially when making this comparison below p_{CO_2} corresponding to a 60:40 CO_2: H_2 mole ratio. Lowering of the overpotential loss for Pt compared to Pt alloys at current densities lower than 0.5 A cm^{-2} has been ascribed to differences inherent to the Pt surface, most likely due to surface electron density. This is the subject of a more detailed investigation in Part II of this report.

Correlation of the overpotential losses as a function of Pt: Mo atomic ratio shows marked differences based on the available Pt surface relative to Mo. An increase in the Pt: Mo atomic ratio results in progressively larger losses in anodic overpotential with 5:1 Pt: Mo ratio showing characteristics close to unalloyed Pt. Comparison of PtMo and PtRu with a nominal 1:1 atomic ratio show remarkably close values for overpotential losses. As expected the results for the 3:1 Pt: Mo atomic ratio fall in between those of 1:1 and 5:1. These results,

however, are true for current densities above 0.5 A cm^{-2}. Below this current density, Pt exhibits better polarization characteristics as discussed in the previous section. These results show that CO_2 and CO tolerance on PtMo follow very different characteristics. Unlike the formation of compact adlayers of CO on the surface, interaction of CO_2 with the surface primarily involves an interaction with adsorbed hydrogen on the surface resulting in possible CO_2–H_2O-clathrate type structures. The need for interaction with surface adsorbed hydrogen to form the reduced CO_2 species results in very different surface requirements, wherein, as is evident from the results of this investigation, the availability of the Pt surface is key. Higher levels of available Pt surface result in greater overpotential loss. In terms of differences with PtRu, the results indicate a very close similarity with PtMo when comparing overpotential losses due to variations in partial pressure of CO_2 for the 1:1 atomic ratio.

Acknowledgements

The authors gratefully acknowledge a grant and materials support from De Nora N.A., E-TEK division, Somerset, NJ. The US Department of Education for graduate assistant support through the GAANN fellowship program is gratefully acknowledged as well as Northeastern University for providing the start-up grant and the necessary infrastructure support.

References

[1] S.G. Chalk, J.F. Miller, F.W. Wagner, J. Power Sources 86 (2000) 40.
[2] H.P. Dhar, L.G. Christner, A.K. Kush, H.C. Maru, J. Electrochem. Soc. 133 (1986) 1574.
[3] J. Giner, Electrochim. Acta 8 (1963) 857.
[4] J. Giner, Electrochim. Acta 9 (1964) 63.
[5] S.B. Brummer, K. Cahill, J. Electroanal. Chem. 21 (1969) 463.
[6] V.N. Kamath, H. Lal, J. Electroanal. Chem. 19 (1968) 137.
[7] P. Stonehart, Electrochim. Acta 18 (1973) 63.
[8] J. Sobkowski, A. Czerwinski, J. Phys. Chem. 89 (1985) 365.
[9] B. Beden, A. Bewick, C. Lamy, J. Electroanal. Chem. 148 (1983) 147.
[10] B. Beden, C. Lamy, J. Electroanal. Chem. 148 (1983) 147.
[11] C. Lamy, J.M. Leger, J. Clavilier, R. Parsons, J. Electroanal. Chem. 150 (1983) 71.
[12] J. Sobkowski, A. Czerwinski, J. Electroanal. Chem. 55 (1974) 391.
[13] J. Sobkowski, A. Czerwinski, J. Electroanal. Chem. 65 (1975) 327.
[14] A. Czerwinski, J. Sobkowski, J. Electroanal. Chem. 59 (1975) 41.
[15] M. Wilson, C. Derouin, J. Valerio, S. Gottesfeld, Proc. Intersoc. Energy Convers. Eng. Conf. 1 (1993) 1203.
[16] S. Swathirajan, Fuel Cell Seminar Extended Abstracts, 1994, p. 204.
[17] S. Kocha, A. Gaskins, P. Plasse, D. Wheeler, Proc. Am. Chem. Soc. 44 (1999) 972.
[18] A.G. Gunner, T.I. Hyde, R.J. Potter, D. Thompsett, US Patent 5,939,220 (1999).
[19] S.J. Cooper, A.G. Gunner, G. Hoogers, D. Thompsett, New Materials for Fuel Cell and Modern Battery Systems II, Proceedings of the International Symposium on New Materials for Fuel Cell and Modern Battery Systems, 2nd, Montreal, 6–10 July, 1997, p. 286.
[20] S. Ball, A. Hodgkinson, G. Hoogers, S. Maniguet, D. Thompsett, B. Wong, Electrochem. Solid-State Lett. 5 (2002) A31.
[21] S. Mukerjee, S.J. Lee, E.A. Ticianelli, J. McBreen, B.N. Grgur, N.M. Markovic, P.N. Ross, J.R. Giallombardo, E.S. De Castroc, Electrochem. Solid-State Lett. 2 (1999) 12.
[22] B.N. Grgur, N.M. Markovic, P.N. Ross, J. Electrochem. Soc. 146 (1999) 1613.
[23] S. Mukerjee, S. Srinivasan, M.P. Soriaga, J. McBreen, J. Electrochem. Soc. 142 (1995) 1409.
[24] J. McBreen, S. Mukerjee, J. Electrochem. Soc. 142 (1995) 3399.
[25] S. Mukerjee, R.C. Urian, C.K. Witham, T.I. Valdez, S.R. Narayanan, Proc. Electrochem. Soc. 4 (2001) 136.
[26] T.E. Springer, T. Rockward, T.A. Zawodzinski, S. Gottesfeld, J. Electrochem. Soc. 148 (2001) A11.
[27] S. Mukerjee, J. McBreen, J. Electrochem. Soc. 143 (1996) 2285.
[28] S. Mukerjee, R.C. Urian, Electrochim. Acta 47 (2002) 3219.
[29] H. Kimura, Trans. Natl. Res. Inst. Metals (Tokyo) 2 (1960) 30.
[30] H. Nishimura, H. Kimura, Nippon Kinzoku Gakkaishi 23 (1959) 616.
[31] A.G. Knapton, J. Inst. Metals 87 (1958) 28.
[32] S.J. Lee, S. Mukerjee, E.A. Ticianelli, J. McBreen, Electrochim. Acta 44 (1999) 3283.
[33] S. Mukerjee, E.A. Ticianelli, S.J. Lee, J. McBreen, J.R. Giallombardo, E.A DeCastro, in: S. Gottesfeld, T.F. Fuller, G. Helpert (Eds.), Meeting of the Electrochemical Society, vols. 98-2, Electrochemical Society, Boston, MA, 1998.
[34] G.A. Camara, E.A. Ticianelli, S. Mukerjee, S.J. Lee, J. McBreen, J. Electrochem. Soc. 149 (2002) A748.
[35] R. Ianniello, V.M. Schmidt, U. Stimming, J. Stumper, A. Wallu, Electrochim. Acta 39 (1994) 1863.
[36] B.N. Grgur, G. Zhuang, N.M. Markovic, P.N. Ross, J. Phys. Chem. 101 (1997) 3910.
[37] H.P. Dhar, L.G. Christner, A.K. Kush, H.C. Maru, J. Electrochem. Soc. 133 (1986) 1574.
[38] J. Sobkowski, A. Czerwinski, J. Phys. Chem. 89 (1985) 365.
[39] S. Taguchi, A. Aramata, M. Enyo, J. Electroanal. Chem. 372 (1994) 161.
[40] S. Taguchi, T. Ohmori, A. Aramata, M. Enyo, J. Electroanal. Chem. 369 (1994) 199.
[41] D.C. Papageorgopoulos, F.A. De Bruijn, J. Electrochem. Soc. 149 (2002) A140.
[42] M.L. Marcos, J.M. Vara, J. Gonzalez-Velasco, A.J. Arvia, J. Electroanal. Chem. 224 (1987) 189.
[43] M.L. Marcos, J. Gonzalez-Velasco, J.M. Vara, M.C. Giordano, A.J. Arvia, J. Electroanal. Chem. 270 (1989) 205.
[44] M.L. Marcos, J. Gonzalez-Velasco, J.M. Vara, M.C. Giordano, A.J. Arvia, J. Electroanal. Chem. 287 (1990) 99.
[45] Y. Hori, H. Wakebe, T. Tsukamoto, O. Koga, Electrochim. Acta 39 (1994) 1833.
[46] N. Hoshi, Y. Hori, Electrochim. Acta 45 (2000) 4263.